Magnetoelectric effect in simple collinear antiferromagnetic spinels

Rana Saha,[1] Somnath Ghara,[1] Emmanuelle Suard,[2] Dong Hyun Jang,[3] Kee Hoon Kim,[3,*]
N. V. Ter-Oganessian,[4,†] and A. Sundaresan[1,‡]

[1]*Chemistry and Physics of Materials Unit and International Centre for Materials Science, Jawaharlal Nehru Centre for Advanced Scientific Research, Jakkur P.O., Bangalore 560 064, India*

[2]*Institut Laue-Langevin, 71 avenue des martyrs, 38042 Grenoble CEDEX, France*

[3]*Center for Novel States of Complex Materials Research (CeNSCMR), Department of Physics and Astronomy, Seoul National University, Seoul 151-747, Republic of Korea*

[4]*Institute of Physics, Southern Federal University, Rostov-on-Don 344090, Russia*

(Received 5 May 2016; revised manuscript received 12 June 2016; published 20 July 2016)

We report the discovery of the linear magnetoelectric effect in a family of spinel oxides, Co_3O_4 and MnB_2O_4 (B = Al, Ga) with simple collinear antiferromagnetic spin structure. An external magnetic field induces a dielectric anomaly at T_N, accompanied by the generation of electric polarization that varies linearly with magnetic field. Magnetization and magnetoelectric measurements on a single crystal of $MnGa_2O_4$ together with a phenomenological theory suggest that the easy axis direction is [111] with the corresponding magnetic symmetry $R\bar{3}'m'$. The proposed theoretical model of single-ion contribution of magnetic ions located in a noncentrosymmetric crystal environment stands for a generic mechanism for observing magnetoelectric effects in these and other similar materials.

DOI: 10.1103/PhysRevB.94.014428

I. INTRODUCTION

Since the pioneering work of Dzyaloshinskii on the prediction of magnetoelectric effect in Cr_2O_3 followed by its experimental observation by Astrov and Rado, the research on magnetoelectric materials continues to grow [1–4]. In linear magnetoelectric material, the cross coupling between magnetic and electric order parameters ($P_i = a_{ij}H_j$ or $M_i = a_{ji}E_j$) provides an additional degree of freedom, which is promising to design novel devices [5,6]. However, the magnetoelectric materials are limited by symmetry requirements, where both spatial inversion and time reversal symmetry need to be broken simultaneously [7]. There are two classes of materials; one exhibits linear magnetoelectric effects without spontaneous electric polarization as observed in materials such as Cr_2O_3 [8], $MnTiO_3$ [9], $NdCrTiO_5$ [10], and $Co_4Nb_2O_9$ [11]. In the second class, a large magnetoelectric effect has been reported in multiferroic materials such as $TbMnO_3$ [12], RMn_2O_5 [13], and $GdFeO_3$ [14], where a spontaneous polarization appears upon magnetic ordering. At room temperature the magnetoelectric effect is found only in few materials, e.g., $BiFeO_3$ and Z-type hexaferrite ($Sr_3Co_2Fe_{24}O_{41}$) [15,16].

Materials belonging to the spinel structure (AB_2O_4) exhibit diverse magnetic properties due to the fact that both the A and the B sublattices can accommodate magnetic ions with various exchange paths between them. However, only a few compounds in the spinel family, e.g., $CoCr_2O_4$ [17] and $ZnCr_2Se_4$ [18], are known to exhibit magnetoelectric properties, including the celebrated compound Fe_3O_4 [19]. $CoCr_2O_4$ is magnetoelectric multiferroic, in which a conical spin ordering gives rise to spontaneous electric polarization, whereas $ZnCr_2Se_4$ exhibits a proper screw spin structure without spontaneous polarization, which can be induced by the application of an external magnetic field. Both compounds show magnetoelectric properties at temperatures below 25 K. Therefore, exploring new magnetoelectric materials, especially in such rich magnetic compounds with crystallographic class as spinels, would help in understanding different microscopic mechanisms, which in turn will lead to the identification of materials with large magnetoelectric coupling.

Spinel compounds with magnetic ions present at the A-site exhibit a plethora of magnetic phenomena, such as spin liquid, orbital liquid, or orbital glass, due to frustration pertinent to the A-site diamond lattice with nearest- and next-nearest-neighbor couplings [20–22]. However, some such spinels show long-range antiferromagnetic order. Herein, we report the experimental confirmation of theoretical predictions of the linear magnetoelectric effect in a family of A-site collinear antiferromagnetic spinel oxides, Co_3O_4, $MnGa_2O_4$, and $MnAl_2O_4$ [23,24]. The symmetry analysis suggests that only single-ion effects can account for magnetoelectric coupling in these spinels [23], i.e., electron orbitals of the ions at the A-sites have spin-dependent electric dipole moments inducing electric polarization in the antiferromagnetic structure. This discovery also provides a new way to manipulate the magnetic state in frustrated A-site magnetic spinels by electric field.

II. EXPERIMENT

A. Polycrystalline sample preparation and structure analysis

Polycrystalline samples of A-site magnetic spinel, MnB_2O_4 (B = Al, Ga) were prepared by conventional solid state reactions starting from the binary oxides, namely, MnO (reduced from Mn_2O_3, Sigma Aldrich, 99%), Al_2O_3 (Alfa Aesar, 99.99%), and Ga_2O_3 (Sigma Aldrich, 99.99%). The stoichiometric amounts of precursors were mixed, ground, and heated in evacuated quartz ampoules at 900 °C and 1000 °C for 24 h. Then the powders were reground, pelletized, and sintered

*optopia@snu.ac.kr
†nikita.teroganessian@gmail.com
‡Corresponding author: sundaresan@jncasr.ac.in

in evacuated quartz ampoules at 1100 °C for 24 h followed by cooling at the rate of 1 °C/min. Also $MnAl_2O_4$ samples under different cooling rates (0.2 and 5 °C/min) were prepared from the sintering temperature of 1100 °C. It is important to mention that the disorder can be controlled by different cooling rates and this disorder significantly affects the properties of this *A*-site magnetic spinel. To prepare Co_3O_4, commercially available Co_3O_4 (Alfa Aesar, 99.7%) was ground, pelletized, and sintered in air at 800 °C for 24 h followed by cooling at a rate of 1 °C/min. Phase purities of all these samples were confirmed by recording x-ray diffraction patterns with a PANalytical Empyrean diffractometer using Cu $K\alpha_1$ monochromatic x-ray radiation. A temperature-dependent neutron diffraction experiment was carried out on the D2B diffractometer at the Institut Laue-Langevin using wavelengths of 1.594 Å. A software package, FULLPROF suite [25], was used for the treatment of diffraction pattern and Rietveld analysis.

B. Single crystal growth, characterization, and measurements

Single-crystalline $MnGa_2O_4$ was grown in three steps by using the floating zone method. First, to make MnO powder, $MnCO_3$ (from Alfa Aesa 99.9%) powder was heated from room temperature to 1100 °C for 12 h in a H_2/Ar mixed gas flow. Second, a $MnGa_2O_4$ polycrystalline sample was prepared by mixing MnO and Ga_2O_3 (from Alfa Aesa 99.99%) powder in a stoichiometric ratio and heated at 1100 °C for 24 h in the same atmosphere. Third, the obtained polycrystalline sample was pressed to make the seed and the feed rods, and melted by infrared image furnace (SC2-MDH, NEC Machinery Co.). A single crystal of $MnGa_2O_4$ was successfully grown at a 5 mm/h growth rate and Ar atmosphere and the molten zone of the sample was found to become stable during the growth. The quality of the single crystal was confirmed by a high resolution x-ray diffraction method (HRXRD, Empyrean, PANalytical) with a Cu $K\alpha_1$ source ($\lambda = 1.540$ Å) to be stoichiometric single phase.

To measure electric polarization, a single-crystalline sample was cut into a cubic shape to remove shape anisotropy effect and electrical contacts were made by silver epoxy on both sides of the sample. Temperature was controlled using a physical property measurement system (PPMS, Quantum Design) and electric polarization was obtained by integrating pyrocurrent using an electrometer (KE617, Keithley). The sample was cooled to 2 K applying a 90 kOe magnetic field and a 1.27 kV cm^{-1} electric field. The electric field was turned off after reaching minimum temperature and then the temperature was warmed up with a temperature sweep rate of 10 K/min. Magnetization was obtained using the vibrating sample magnetometer (PPMS-VSM, Quantum Design) equipped in the PPMS.

C. Measurements on polycrystalline samples

dc magnetization measurements were carried out using a superconducting quantum interference device magnetometer (SQUID, MPMS3, Quantum Design) in the temperature range of 2–390 K. The specific heat (C_p) was measured while cooling the sample from the temperature above T_N in a PPMS (Quantum Design). To measure the capacitance and the pyroelectric current an *LCR* meter (Agilent E4980A) and an electrometer (Keithley 6517A), respectively, were used using a multifunction probe inserted in the PPMS which allowed one to access the temperature and the magnetic field. The electrode was made by applying the conducting Ag paint on both sides of the thin pellets and dried under an infrared lamp. The capacitance was measured in the presence of a magnetic field while warming after performing the field cooling of the sample from above T_N. Before measuring the pyroelectric current, the sample was poled magnetoelectrically while cooling from a temperature above T_N and then short circuited for 15 min to remove any charges related to the leakage current, but the magnetic field was not removed. After that, magnetoelectric current was measured on warming the sample to a temperature above T_N at a rate of 8 K/min (for Co_3O_4) and 15 K/min (for $MnGa_2O_4$ and $MnAl_2O_4$) while the magnetic field was kept applied on the sample. The electric polarization was obtained by integrating the magnetoelectric current with respect to time and dividing it by the area of the sample after performing necessary background subtraction. dc voltage was applied on the samples by using a Radiant Technologies, Inc. precision workstation. The onset temperature of magnetoelectric polarization is a little higher as compared to the phase transition temperature determined from magnetic or dielectric measurements due to the high ramping rate used for recording the pyroelectric current while warming.

III. RESULTS AND DISCUSSION

Co_3O_4 and MnB_2O_4 (B = Al, Ga) crystallize in the normal spinel structure with the space group $Fd\bar{3}m$ [Fig. 1(a)], where Co^{2+} (Mn^{2+}) ions occupy the tetrahedral sites ($8a$) and the nonmagnetic Co^{3+} (B^{3+}) ions (S = 0) occupy the octahedral ($16d$) sites. The weak magnetic interactions among Co^{2+}/Mn^{2+} ions at the tetrahedral sites result in a collinear antiferromagnetic ordering at low temperatures (<40 K) [26,27]. Rietveld analysis of the room temperature neutron diffraction data [Supplemental Material, Fig. S1(a)] of polycrystalline $MnGa_2O_4$ reveals the occurrence of a small amount of cation inversion between the *A* and *B* sites [Supplemental Material, Table SI] [28]. The presence of the (200) magnetic Bragg peak in the neutron diffraction pattern of $MnGa_2O_4$ acquired at 3.5 K [Supplemental Material, Fig. S1(b)] confirms the long-range antiferromagnetic ordering of Mn^{2+} spins. Co_3O_4 is characterized by a similar antiferromagnetic ordering of Co^{2+} spins [29]. Because of the polycrystalline nature of the sample and cubic structure, it is not possible to distinguish between the two probable magnetic easy axes [100]/[111], as shown in Figs. 1(b) and 1(c), which correspond to the magnetic space group symmetries $I4'_1/a'm'd$ and $R\bar{3}'m'$, respectively, and both of them allow the linear magnetoelectric effect. Thus, in earlier studies on polycrystalline $MnAl_2O_4$, Co_3O_4, and $MnGa_2O_4$ it was not possible to determine the easy axis direction contrary to what is claimed in some works [27,29,30]. Correct determination of the easy axis is important to understand the magnetic symmetry governing the magnetoelectric interaction in this family of oxides. Therefore, in this work, based on the magnetic and magnetoelectric measurements on single-crystalline $MnGa_2O_4$, we could distinguish the actual

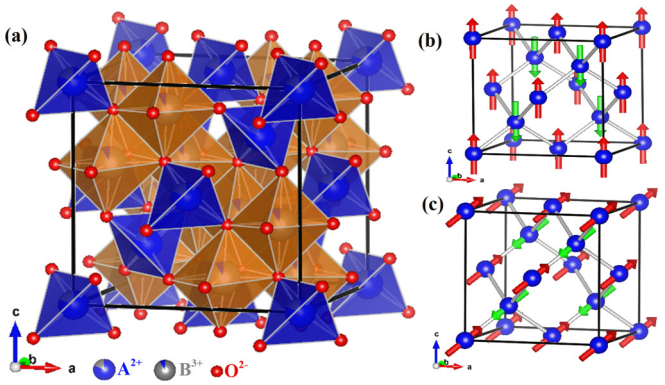

FIG. 1. (a) Schematic representation of cubic crystal structure of A-site magnetic spinel oxide (AB_2O_4). Magnetic structures of $MnGa_2O_4$ with spin moments along (b) [001] and (c) [111] directions.

direction of easy axis to be [111]. Since we obtained a similar magnetoelectric effect in $MnAl_2O_4$, we provide corresponding results in the Supplemental Material [28]. The origin of the magnetoelectric effect in this family of spinel oxides has been discussed in the light of symmetry and group theoretical analysis.

Temperature-dependent dc magnetization, M (T) for Co_3O_4 and $MnGa_2O_4$ measured in the presence of a magnetic field of 1 kOe under field cooled condition, are shown in Figs. 2(a) and 2(b), respectively. From the magnetization data, it is clear that both Co_3O_4 and $MnGa_2O_4$ undergo antiferromagnetic ordering at 30 and 32 K, respectively. However, there is a marked difference in the magnetization behavior of these two samples. It is important to note that the M (T) curve of Co_3O_4 shows a maximum at T_N, while in $MnGa_2O_4$ the M (T) curve shows a steep increase below the antiferromagnetic transition. The decrease of M (T) below T_N in Co_3O_4 is consistent with conventional antiferromagnetic ordering, whereas the increase of M (T) below T_N for $MnGa_2O_4$ is due to the paramagnetic moment of Mn^{2+} arising from antisite disorder between the A and B sites [31]. This observation is consistent with the Rietveld analysis of the room temperature neutron diffraction data where we see an inversion parameter (α) of 0.095 as defined in the Supplemental Material [28].

The temperature-dependent inverse susceptibility data of Co_3O_4 could be fitted with the Curie-Weiss law [$\chi = \frac{C}{T-\theta}$], while in the case of $MnGa_2O_4$ it requires a modified Curie-Weiss law [$\chi = \frac{C}{T-\theta} + \frac{C'}{T}$] to take into account the presence of paramagnetic Mn^{2+} ions (9.5%) in the octahedral site [30] as shown in the Supplemental Material, Figs. S2(a) and S2(b) [28]. From the above-mentioned fitting in the temperature range of 200–390 K, we obtain the effective magnetic moment (μ_{eff}) of 4.8 μ_B per Co^{2+} ion for Co_3O_4, and 5.65 and 1.51 μ_B per Mn^{2+} ion for $MnGa_2O_4$ in the tetrahedral and octahedral sites, respectively. Despite the differences in the magnetization data, the specific heat data of both the compounds show the λ-shape anomaly at the respective magnetic transitions, corroborating the long-range, second order antiferromagnetic phase transition [inset of Figs. 2(a) and 2(b)]. Isothermal magnetization data recorded at 2 K, as shown in the Supplemental Material, Figs. S2(c) and S2(d), confirm the antiferromagnetic nature of both these

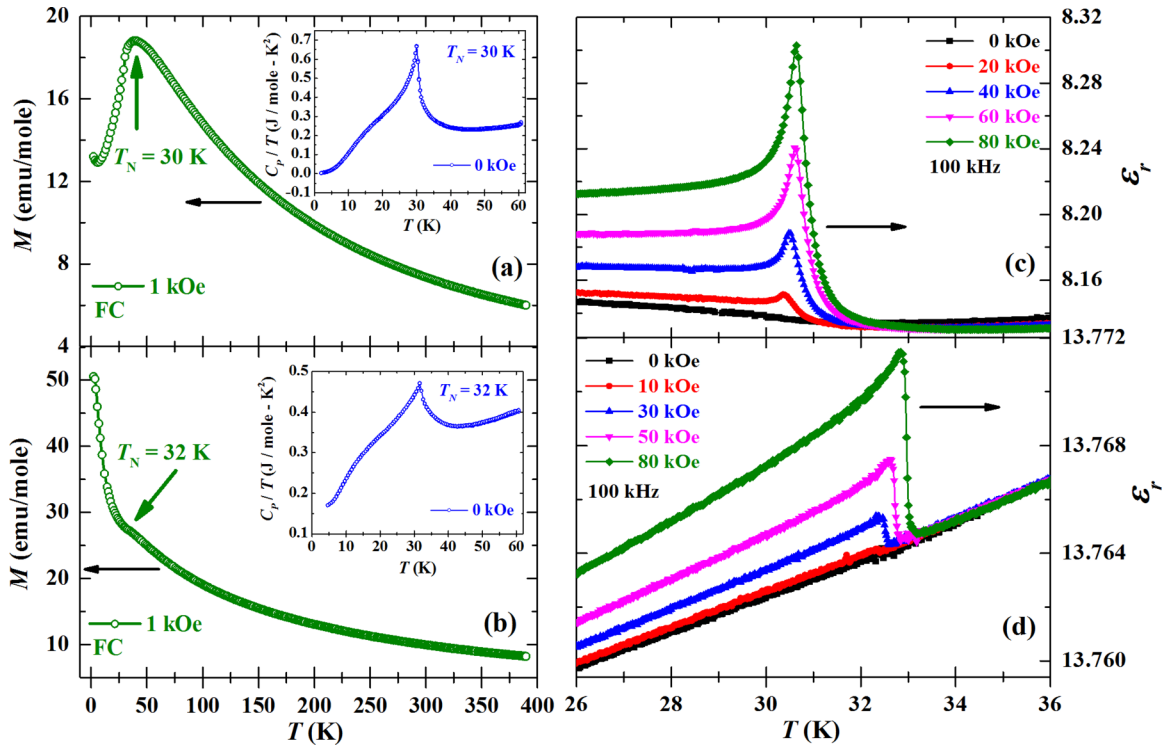

FIG. 2. Temperature dependencies of dc magnetization of (a) Co_3O_4 and (b) $MnGa_2O_4$. Insets of (a) and (b) show the C_p/T as a function of temperature for the respective compounds. Temperature-dependent dielectric constant measured in the presence of different magnetic fields for (c) Co_3O_4 and (d) $MnGa_2O_4$.

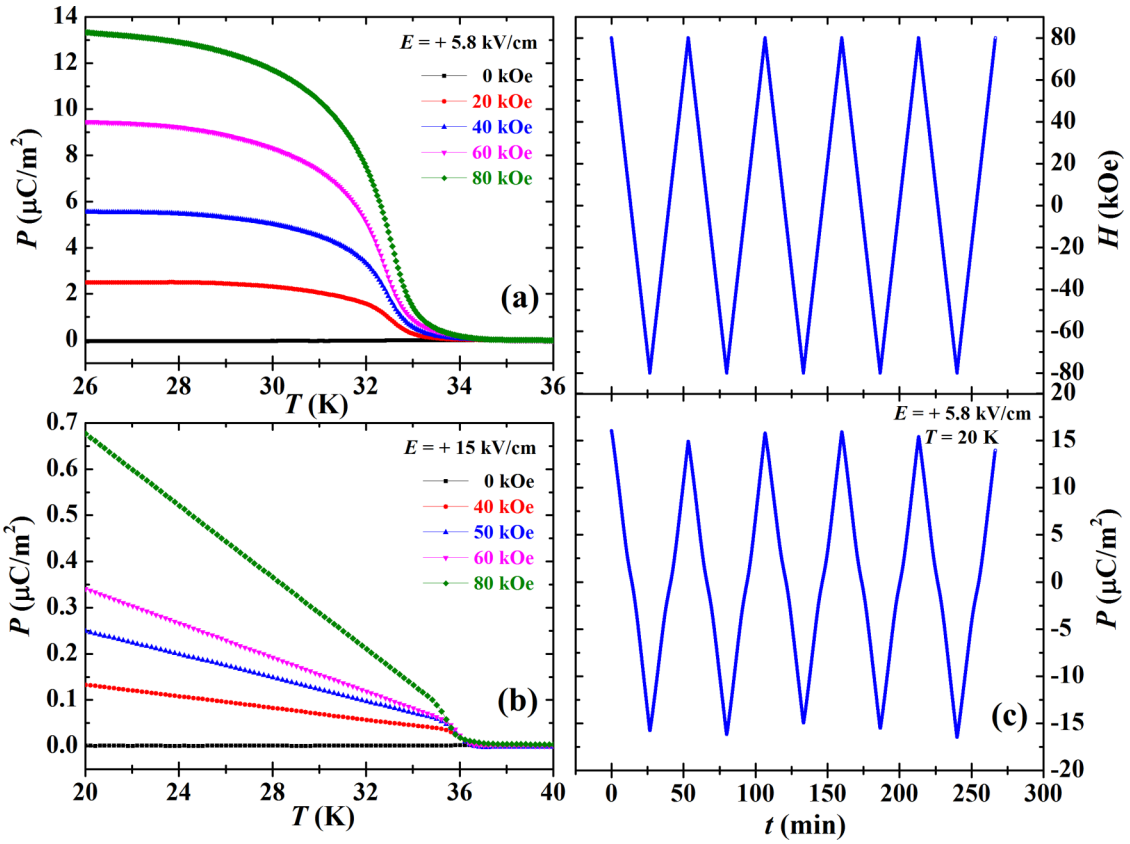

FIG. 3. Temperature-dependent magnetoelectric polarization induced by magnetic field for (a) Co_3O_4 and (b) $MnGa_2O_4$. (c) Switching of magnetoelectric polarization in the presence of an oscillating magnetic field of ±80 kOe for Co_3O_4 at 20 K.

compounds [28]. $MnAl_2O_4$ shows a similar antiferromagnetic phase transition ($T_N = 41$ K) as shown in the Supplemental Material, Figs. S3(a) and S3(b).

The temperature dependence of the real part of the dielectric constant measured at 100 kHz is shown in Figs. 2(c) and 2(d) for Co_3O_4 and $MnGa_2O_4$, respectively. At zero magnetic field, the dielectric constant does not show any peak or anomaly at the magnetic transition temperature. On application of a small magnetic field, a feeble peak feature appears in both these compounds. With increasing the magnitude of the magnetic field, the intensity of the peak becomes more pronounced, demonstrating strong coupling between magnetism and dielectric polarizability. Interestingly, the magnetic-field dependence of the dielectric constant exhibits a strong magnetocapacitance effect, which is maximum near the antiferromagnetic transition [see Supplemental Material, Figs. S4(a) and S4(b)] [28], indicating the origin to be associated with magnetoelectric coupling.

We have carried out pyroelectric current measurements in the presence of various magnetic fields after performing the magnetoelectric poling (both magnetic and electric fields were applied during cooling) from a temperature above T_N. This magnetoelectric annealing condition is essential to realize a single domain state responsible for exhibiting the electric polarization. In Figs. 3(a) and 3(b), we show the temperature-dependent electric polarization for Co_3O_4 and $MnGa_2O_4$ in the presence of different magnetic fields. Electric polarization appears at the magnetic ordering temperature, where the dielectric anomaly also appears, only when the external magnetic field is applied. It is clear from these data, that with increasing magnitude of magnetic field, electric polarization is enhanced, which signifies the critical role of the magnetic field to induce electric polarization. The proportionality between external magnetic field and magnetoelectric polarization indicates the linear nature of the magnetoelectric effect.

From the temperature and magnetic-field dependent electric polarization data, we calculated the magnetoelectric coefficients at 20 K for Co_3O_4 (2.6 ps/m at $E = 5.8$ kV/cm) and $MnGa_2O_4$ (0.17 ps/m at $E = 15$ kV/cm), which are comparable to the polycrystalline linear magnetoelectric material $NdCrTiO_5$ (0.54 ps/m at 16 K in the presence of $E = 5.8$ kV/cm, $H = 70$ kOe) [10]. $MnAl_2O_4$ shows similar magnetic-field induced dielectric and ferroelectric phase transitions in the magnetically ordered state [Supplemental Material, Figs. S5(a)–S5(c)]. The magnetoelectric coefficient for $MnAl_2O_4$ is 0.13 ps/m ($T = 30$ K, $E = 22.3$ kV/cm, $H = 80$ kOe). To demonstrate the synchronized reversal of magnetoelectric polarization with magnetic fields, a sequential scan of magnetic fields was carried out between +80 and −80 kOe in Co_3O_4 as shown in Fig. 3(c). This figure further confirms that magnetoelectric polarization varies linearly with the external magnetic field indicating direct coupling between electric polarization and magnetic fields.

In the absence of neutron diffraction experiment, we have performed magnetic and magnetoelectric measurements on a single crystal of $MnGa_2O_4$ to determine the easy axis. The

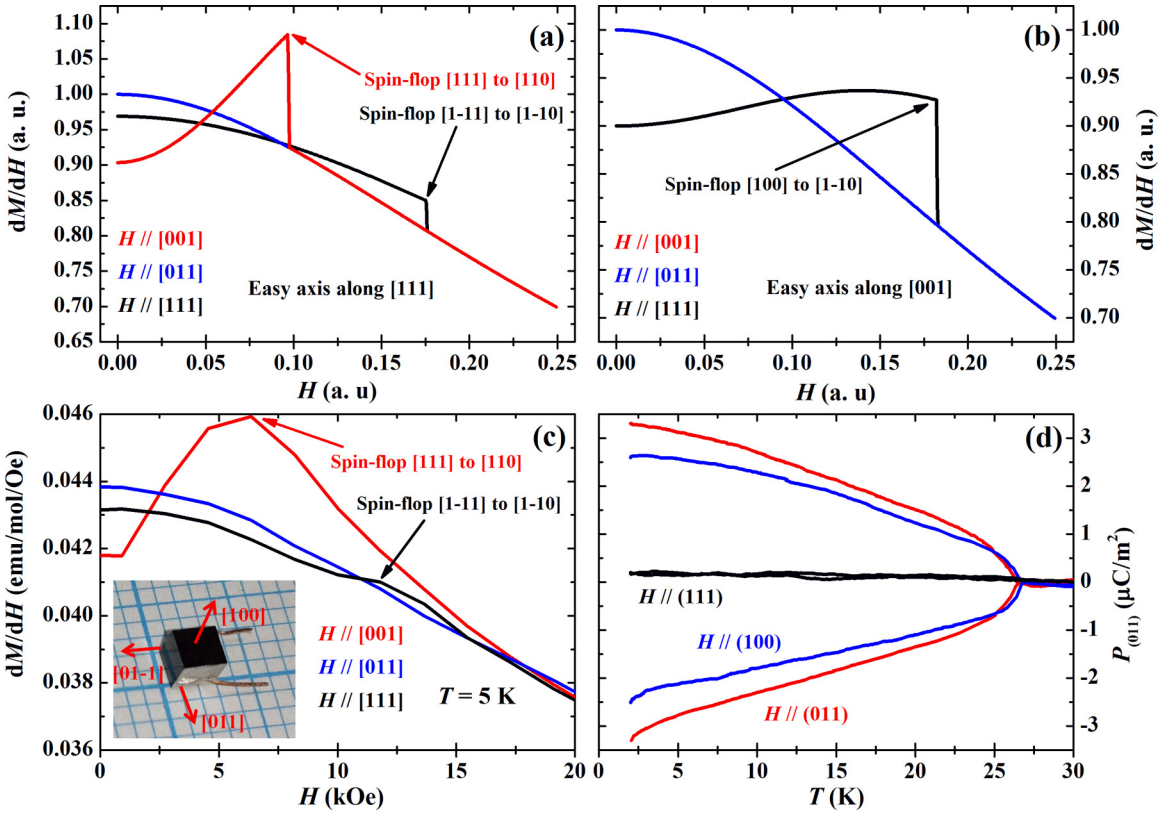

FIG. 4. Theoretically calculated magnetic-field dependent $dM(H)/dH$ in $MnGa_2O_4$ for the easy axis along (a) [111] and (b) [001] directions. (c) Magnetic-field dependent $dM(H)/dH$ measured along [001], [011], and [111] on a single crystal of $MnGa_2O_4$. Inset of (c) shows the crystal of $MnGa_2O_4$. (d) Temperature-dependent magnetic field ($H = 90$ kOe) induced electric polarization along [011] with $H\|[100]$, $H\|[011]$, $H\|[111]$ on a single crystal of $MnGa_2O_4$.

magnetic and magnetoelectric properties in the studied materials can be understood using the phenomenological theory of phase transitions. The A-site collinear antiferromagnetic structure for $\vec{k} = 0$ in spinels corresponds to the irreducible representation Γ^{5-} and can be described by the order parameter (L_x, L_y, L_z). Here, we use the orthogonal axes x, y, and z, which are aligned along the cubic edges. One can write the thermodynamic potential expansion in the form

$$\Phi_{\text{magn}} = \frac{A}{2} I_1 + \frac{B_1}{4} I_2 + \frac{B_2}{4} I_1^2 + \frac{C}{6} I_1^3 + f I_{ML} + \frac{\alpha}{2} I_M + \frac{\beta}{2} I_M^2 - \vec{H}\vec{M}, \quad (1)$$

where A, B_1, B_2, C, f, α, and β are phenomenological coefficients, $\vec{M}$ is the magnetic moment, $I_1 = L_x^2 + L_y^2 + L_z^2$, $I_2 = L_x^4 + L_y^4 + L_z^4$, $I_{ML} = (L_x M_x + L_y M_y + L_z M_z)^2$, and $I_M = M_x^2 + M_y^2 + M_z^2$. The term I_{ML} in the expansion determines the interaction between $\vec{L}$ and $\vec{M}$ favoring their perpendicularity when $f > 0$ and governs the spin-flop behavior as discussed below. The easy axis directions [111] or [100] are obtained, when $B_1 > 0$ or $B_1 < 0$, respectively. Performing numerical minimization of the functional (1) we obtain the $dM(H)/dH$ dependencies as shown in Figs. 4(a) and 4(b). It can be seen that the easy axes along [111] and [001] have qualitatively different $dM(H)/dH$ curves with different spin-flop phase transitions. For the easy axis along [111] [Fig. 4(a)], the anomalies of $dM(H)/dH$ curves that correspond to spin flops, their amplitudes and succession as well as the succession of curves at $H = 0$ qualitatively agree with the measurements on the single crystal of $MnGa_2O_4$ [Fig. 4(c)]. In Fig. 4(c), we show the magnetic-field dependence of $dM(H)/dH$ at 5 K measured along three different directions. We see an anomaly in the data at $H \sim 6$ kOe when the magnetic field is applied along [001] and another anomaly at ~11 kOe when the magnetic field is applied along [111]. We do not observe any such anomaly when the magnetic field was applied along the [011] direction. Such behavior is in accordance with the theoretical calculations of Fig. 4(a) and therefore, we attribute these anomalies in the dM/dH vs H plots to the spin-flop transitions, in which the antiferromagnetic vector wants to orient perpendicular to the direction of the applied field. In $MnGa_2O_4$, an anomaly at ~6 kOe in magnetic-field dependence of the (200) magnetic reflection in neutron scattering was also found earlier [30], which was also associated with the spin-flop transition.

The measurements of magnetic-field induced polarization can also give hints on the easy axis direction. Consider the thermodynamic potential with magnetoelectric interaction

$$\Phi = \Phi_{\text{magn}} + \kappa I_{ME} + \frac{a}{2} I_P, \quad (2)$$

where a and κ are phenomenological coefficients, $\vec{P}$ is the electric polarization, $I_P = P_x^2 + P_y^2 + P_z^2$, and the magnetoelectric interaction can be written in the form [23]

$$I_{ME} = L_x(M_y P_z + M_z P_y) + L_y(M_z P_x + M_x P_z) + L_z(M_x P_y + M_y P_x). \quad (3)$$

Due to the presence of spin-flop transitions with rather low critical magnetic-field values H_c, at which the antiferromagnetic vector aligns perpendicular to the applied magnetic field, the easy axis directions [100] and [111] in $MnGa_2O_4$ give similar magnetoelectric responses for $H > H_c$ for any chosen geometry, whereas for $H < H_c$, induced electric polarization cannot be measured reliably. However, it follows from Eq. (2) that at high magnetic fields (i.e., magnetic fields higher than spin-flop magnetic-field values) the ratio of $P||[011]$ at $H||[011]$ to $P||[011]$ at $H||[100]$ is different for the easy axis directions [001] and [111]. When the easy axis direction is parallel to [001] the ratio is $2\sqrt{2}$, whereas for the direction parallel to [111] it is $\sqrt{2}$. We have measured temperature-dependent electric polarization in the presence of a magnetic field of 90 kOe applied to different directions of the $MnGa_2O_4$ single crystal as shown in Fig. 4(d). From this measurement, we see that the ratio of $P\|[011]$ at $H\|[011]$ to $P\|[011]$ at $H\|[100]$ is 1.3 at 2 K ($E = 1.27\,\mathrm{kV/cm}$, $H = 90\,\mathrm{kOe}$), which is close to $\sqrt{2}$. Hence, the magnetic and magnetoelectric measurements interpreted by the phenomenological theory of phase transitions confirm that easy axis of $MnGa_2O_4$ is [111].

The interaction described by Eq. (3) results in a linear coupling between $\vec{M}$ and $\vec{P}$ upon a phase transition into the antiferromagnetic phase, which implies the appearance of the linear magnetoelectric effect. A qualitative description of the phase transitions and a comparison of magnetically induced electric polarization with the experiment [Supplemental Material, Figs. S6(a) and S6(b)] is performed in the Supplemental Material [28].

In order to understand the microscopic mechanism behind the linear magnetoelectric effect, we can rewrite the interaction I_{ME} in terms of the spins of the A and B ions. Each primitive unit cell contains two A ions located at $(\frac{1}{8},\frac{1}{8},\frac{1}{8})$ and $(\frac{7}{8},\frac{7}{8},\frac{7}{8})$ and four B ions located at $(\frac{1}{2},\frac{1}{2},\frac{1}{2})$, $(\frac{1}{2},\frac{3}{4},\frac{3}{4})$, $(\frac{3}{4},\frac{1}{2},\frac{3}{4})$, and $(\frac{3}{4},\frac{3}{4},\frac{1}{2})$. Their respective spins can be denoted by $\vec{S}_{Ai}$ $(i = 1,2)$ and $\vec{S}_{Bj}$ $(j = 1,2,3,4)$. The antiferromagnetic order parameter can be written as $\vec{L} = \vec{S}_{A1} - \vec{S}_{A2}$, whereas the contributions of the A and B ions to magnetic moment can be written as $\vec{M}_A = \vec{S}_{A1} + \vec{S}_{A2}$ and $\vec{M}_B = \vec{S}_{B1} + \vec{S}_{B2} + \vec{S}_{B3} + \vec{S}_{B4}$, respectively. Using $\vec{M}_A$ and $\vec{M}_B$ instead of $\vec{M}$ in (3), we obtain the magnetoelectric interactions

$$2P_x(S_{A1y}S_{A1z} - S_{A2y}S_{A2z}) + 2P_y(S_{A1x}S_{A1z} - S_{A2x}S_{A2z}) + 2P_z(S_{A1x}S_{A1y} - S_{A2x}S_{A2y}) \quad (4)$$

and

$$\sum_{j=1,2,3,4} (\vec{S}_{A1} \otimes \vec{S}_{Bj} - \vec{S}_{A2} \otimes \vec{S}_{Bj})\vec{P}, \quad (5)$$

respectively. Here $\otimes$ denotes $\vec{V}_1 \otimes \vec{V}_2 = (V_{1y}V_{2z} + V_{1z}V_{2y}; V_{1z}V_{2x} + V_{1x}V_{2z}; V_{1x}V_{2y} + V_{1y}V_{2x})$. Interaction (4) is due to single-ion effects at the A sites, whereas Eq. (5) stems from the interaction between the A and B ions, which is not of the form $\vec{P} \sim [\vec{S}_{Ai} \times \vec{S}_{Bj}]$ generally used for the description of magnetoelectric polarization.

In all the materials investigated in the present study, only the ions Co^{2+} and Mn^{2+} located at the A site possess magnetic moments. Therefore, electric polarization in these spinels can only be induced by single-ion effects according to Eq. (4), which we estimate in the Supplemental Material [28] using the model suggested in the literature [24] resulting in the values $1-10\,\mu\mathrm{C\,m^{-2}}$ for Co_3O_4 and $0.1-1\,\mu\mathrm{C\,m^{-2}}$ for $MnGa_2O_4$ and $MnAl_2O_4$ in good agreement with the experiment. In $CoCr_2O_4$ and $ZnCr_2Se_4$ the magnetoelectric effect is assumed to originate from the Dzyaloshinskii-Moriya-type interaction [32]. Our work shows that the single-ion magnetoelectric effect due to spins and electric dipoles in tetrahedral positions is equally important, and may be used for comparison of various microscopic mechanisms of magnetoelectric coupling. Nonmagnetic anions in noncentrosymmetric positions, as in, e.g., $ZnCr_2Se_4$, can also contribute to the magnetoelectric effect as suggested in Ref. [24].

IV. CONCLUSION

In conclusion, we have demonstrated the linear magnetoelectric effect in the A-site magnetic spinels Co_3O_4 and MnB_2O_4 (B = Al, Ga), which are antiferromagnetic insulators. Contrary to many other spinels experiencing structural distortions, these compounds become linear magnetoelectric below a single second order antiferromagnetic phase transition from a highly symmetric cubic structure, which makes them unique. Using magnetic and magnetoelectric measurements, we were able to determine the easy axis direction in $MnGa_2O_4$. Based on the symmetry analysis we showed that the linear magnetoelectric effect is not restricted to the studied compounds, but should pertain also to other A-site antiferromagnetic spinels with $\vec{k} = 0$ such as, for example, $CoRh_2O_4$ and $NiRh_2O_4$. The microscopic symmetry analysis reveals that single-ion contributions are essential to the origin of the magnetoelectric effect in these compounds. The studied compounds can be regarded as some of the few exceptions in the family of spinels with magnetic ions only at the A site, which usually show frustrated magnetism. The discovery of linear magnetoelectricity in them is not only important for the spinel family as a whole, but can also open new physics in the control of frustrated magnetism by electric fields. Due to the presence of spin-dependent electric dipole moments of magnetic ions, the application of an electric field can help in studying the physics of A-site frustrated magnetic spinels including the determination of the ground state.

ACKNOWLEDGMENTS

A.S. would like to acknowledge the financial support from Science and Engineering Research Board (SERB Sanction No. EMR/2014/000896), Department of Science and Technology, Government of India. A. S. would like to acknowledge Sheikh Saqr Laboratory at Jawaharlal Nehru Centre for Advanced Scientific Research for providing experimental facilities. R.S.

and S.G. acknowledge JNCASR for providing a research fellowship. N.V.T. acknowledges the financial support from the SFedU Grant No. 213.01-2014/011-VG. Work at SNU was supported by the National Creative Research Initiatives (Grant No. 2010-0018300).

R.S. and S.G. contributed equally to this work.

[1] I. E. Dzyaloshinskii, Zh. Exp. Teor. Fiz. **37**, 881 (1959) [Sov. Phys. JETP **10**, 628 (1960)].
[2] D. N. Astrov, Sov. Phys. JETP **11**, 708 (1960).
[3] D. N. Astrov, Sov. Phys. JETP **13**, 729 (1961).
[4] G. Rado and V. Folen, Phys. Rev. Lett. **7**, 310 (1961).
[5] M. Fiebig, J. Phys. D: Appl. Phys. **38**, R123 (2005).
[6] J. Scott, J. Mater. Chem. **22**, 4567 (2012).
[7] W. Eerenstein, N. Mathur, and J. F. Scott, Nature (London) **442**, 759 (2006).
[8] A. Iyama and T. Kimura, Phys. Rev. B **87**, 180408 (2013).
[9] N. Mufti, G. R. Blake, M. Mostovoy, S. Riyadi, A. A. Nugroho, and T. T. M. Palstra, Phys. Rev. B **83**, 104416 (2011).
[10] J. Hwang, E. S. Choi, H. D. Zhou, J. Lu, and P. Schlottmann, Phys. Rev. B **85**, 024415 (2012).
[11] Y. Fang, Y. Q. Song, W. P. Zhou, R. Zhao, R. J. Tang, H. Yang, L. Y. Lv, S. G. Yang, D. H. Wang, and Y. W. Du, Sci. Rep. **4**, 3860 (2014).
[12] T. Kimura, T. Goto, H. Shintani, K. Ishizaka, T. Arima, and Y. Tokura, Nature (London) **426**, 55 (2003).
[13] N. Hur, S. Park, P. Sharma, J. Ahn, S. Guha, and S. Cheong, Nature (London) **429**, 392 (2004).
[14] Y. Tokunaga, N. Furukawa, H. Sakai, Y. Taguchi, T.-h. Arima, and Y. Tokura, Nat. Mater. **8**, 558 (2009).
[15] J. Wang *et al.*, Science **299**, 1719 (2003).
[16] Y. Kitagawa, Y. Hiraoka, T. Honda, T. Ishikura, H. Nakamura, and T. Kimura, Nat. Mater. **9**, 797 (2010).
[17] Y. Yamasaki, S. Miyasaka, Y. Kaneko, J.-P. He, T. Arima, and Y. Tokura, Phys. Rev. Lett. **96**, 207204 (2006).
[18] H. Murakawa, Y. Onose, K. Ohgushi, S. Ishiwata, and Y. Tokura, J. Phys. Soc. Jpn. **77**, 043709 (2008).
[19] E. Kita, K. Siratori, K. Kohn, A. Tasaki, S. Kimura, and I. Shindo, J. Phys. Soc. Jpn. **47**, 1788 (1979).
[20] A. Krimmel, H. Mutka, M. M. Koza, V. Tsurkan, and A. Loidl, Phys. Rev. B **79**, 134406 (2009).
[21] V. Fritsch, J. Hemberger, N. Büttgen, E.-W. Scheidt, H.-A. Krug von Nidda, A. Loidl, and V. Tsurkan, Phys. Rev. Lett. **92**, 116401 (2004).
[22] R. Fichtl, V. Tsurkan, P. Lunkenheimer, J. Hemberger, V. Fritsch, H.-A. Krug von Nidda, E.-W. Scheidt, and A. Loidl, Phys. Rev. Lett. **94**, 027601 (2005).
[23] N. V. Ter-Oganessian, J. Magn. Magn. Mater. **364**, 47 (2014).
[24] V. P. Sakhnenko and N. V. Ter-Oganessian, J. Phys.: Condens. Matter **24**, 266002 (2012).
[25] J. Rodríguez-Carvajal, Phys. B (Amsterdam, Neth,) **192**, 55 (1993).
[26] N. Tristan, J. Hemberger, A. Krimmel, H.-A. Krug von Nidda, V. Tsurkan, and A. Loidl, Phys. Rev. B **72**, 174404 (2005).
[27] H. S. Nair, Z. Fu, J. Voigt, Y. Su, and T. Brückel, Phys. Rev. B **89**, 174431 (2014).
[28] See Supplemental Material at http://link.aps.org/supplemental/10.1103/PhysRevB.94.014428 for some useful measurements on magnetic, dielectric, and pyroelectric properties on *A*-site magnetic spinel oxides as well as a phenomenological description of the phase transition and magnetoelectricity.
[29] W. Roth, J. Phys. Chem. Solids **25**, 1 (1964).
[30] B. Boucher, A. Herpin, and A. Oles, J. Appl. Phys. **37**, 960 (1966).
[31] H. Montiel, G. Alvarez, A. Conde-Gallardo, and R. Zamorano, J. Magn. Magn. Mater. **385**, 188 (2015).
[32] I. A. Sergienko and E. Dagotto, Phys. Rev. B **73**, 094434 (2006).